Inorganic Chemistry
Article

Inorg. Chem. **2010**, *49*, 8333–8346 **8333**
DOI: 10.1021/ic1008413

Energy Transfer Dynamics in Multichromophoric Arrays Engineered from Phosphorescent $Pt^{II}/Ru^{II}/Os^{II}$ Centers Linked to a Central Truxene Platform

Barbara Ventura,*,† Andrea Barbieri,† Francesco Barigelletti,† Stéphane Diring,‡ and Raymond Ziessel*,‡

†*Istituto per la Sintesi Organica e la Fotoreattività, Consiglio Nazionale delle Ricerche (ISOF-CNR), Via P. Gobetti 101, 40129 Bologna, Italy, and* ‡*Laboratoire de Chimie Organique et Spectroscopies Avancées (LCOSA), Ecole de Chimie, Polymères, Matériaux (ECPM), Université de Strasbourg (UdS), 25 rue Becquerel, 67087 Strasbourg Cedex 02, France*

Received April 28, 2010

A rigid star-shaped tetrachromophoric trimetallic complex engineered from a 5,5′,10,10′,15,15′-hexabutyltruxene platform functionalized in the 2,7,12 positions with three different metal centers, namely, a terpyridine-Pt(II) ethynylene unit and Ru(II) and Os (II) bipyridine centers, was synthesized in a controlled fashion and characterized by ^{1}H NMR and mass spectrometry. The protocol was devised in such a way that key mono and dinuclear model complexes and two reference truxene ligands could also be prepared. Room temperature (RT) optical absorption and RT and 77 K luminescence studies were performed on the truxene ligands, the trimetallic species, the various mono- and binuclear complexes and precursors lacking the truxene fragment; RT nanosecond transient absorption measurements were also carried out in particular cases. The electronic properties of the Ru and Os subunits in the arrays were found to be unaffected by the presence of the truxene core whereas direct linking of the Pt subunit to the truxene via the σ-alkyne bond markedly influences the spectroscopic behavior of the Pt center. Remarkably the truxene phosphorescence was clearly established in the two ligands (lifetime of 4.3 s for the mono ethynyl-bipy substituted truxene and 17.5 ms for the bis ethynyl-bipy substituted truxene) and also detected in the Pt-containing complexes **PtL′** (model Pt-truxene) and **Pt−Os** (Pt-truxene-Os dyad) at low temperature. This is attributed to the closeness in energy of the Pt ^{3}CT level and the truxene triplet at low temperature and to the spin−orbit coupling induced by the Pt heavy atom. Transient absorbance measurements evidenced the population of the Pt-based triplet in the Pt-truxene mononuclear complex **PtL′** at room-temperature. For the trimetallic complex, where the various centers exhibit an energy gradient for the local excited levels, and following an approach based on the use of selected excitation of the components, an initial energy transfer was found to occur from the central truxene unit toward the peripheral Pt, Ru, and Os metal-based centers. Subsequent Pt-based and Ru-based excited state depletion contributes to the final sensitization of the low-lying Os triplet excited state; the excited state dynamics for these multicascade processes are examined in detail.

Introduction

Light collection in artificial devices is an issue of great relevance for studies of solar energy conversion and molecular scale electronics and photonics.[1] A synthetic antenna should consist in a multichromophoric architecture with large UV−vis absorption cross-section, well-defined spatial orientation of the chromophores, and suitable energy gradients to convey the energy toward a specific site. Dendritic frameworks have been largely explored for the construction of such antenna systems since they allow a site-specific ordering of the dye molecules in space.[2−5]

The choice of the core scaffold for the construction of multichromophoric dendritic architectures is a key task, and the need of modules capable to act as photoactive partners inside the arrays is prompting researchers to explore new building materials and linkers.

Truxene is a planar heptacyclic polyarene system that can formally be regarded as a C_3-symmetrically fused fluorene trimer. The truxene platform can easily be functionalized in three diverging directions in space to serve as an excellent building block for large star-shaped dendritic architectures.[6−8]

*To whom correspondence should be addressed. E-mail: bventura@isof.cnr.it (B.V.), ziessel@unistra.fr (R.Z.).

(1) Balzani, V.; Credi, A.; Venturi, M. *ChemSusChem* **2008**, *1*, 26–58.
(2) Balzani, V.; Ceroni, P.; Maestri, M.; Vicinelli, V. *Curr. Opin. Chem. Biol.* **2003**, *7*, 657–665.
(3) Nantalaksakul, A.; Reddy, D. R.; Bardeen, C. J.; Thayumanavan, S. *Photosynth. Res.* **2006**, *87*, 133–150.
(4) Serin, J. M.; Brousmiche, D. W.; Frechet, J. M. J. *Chem. Commun.* **2002**, 2605–2607.
(5) Cotlet, M.; Vosch, T.; Habuchi, S.; Weil, T.; Mullen, K.; Hofkens, J.; De Schryver, F. *J. Am. Chem. Soc.* **2005**, *127*, 9760–9768.
(6) Cao, X. Y.; Zhang, W. B.; Wang, J. L.; Zhou, X. H.; Lu, H.; Pei, J. *J. Am. Chem. Soc.* **2003**, *125*, 12430–12431.
(7) Cao, X. Y.; Liu, X. H.; Zhou, X. H.; Zhang, Y.; Jiang, Y.; Cao, Y.; Cui, Y. X.; Pei, J. *J. Org. Chem.* **2004**, *69*, 6050–6058.

© 2010 American Chemical Society
Published on Web 08/17/2010

Scheme 1. Synthesis of Ligand **L** and Complexes **OsL** and **RuL**[a]

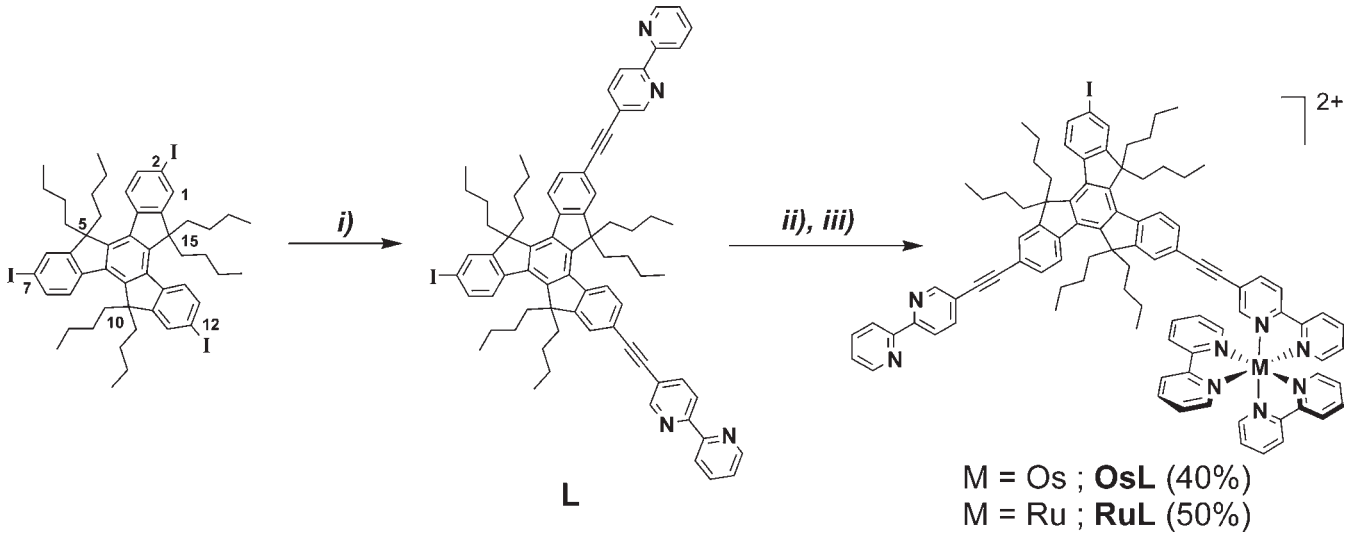

[a] (*i*) 5-ethynyl-2,2′-bipyridine (2 equiv), $[Pd(PPh_3)_4]$ (12%), *n*-propylamine, 60 °C, 18h; (*ii*) M^{II} = Os: $[Os(bpy)_2Cl_2]$ (1 equiv), EtOH, microwave, 1200 W, 180 °C, 1h or M^{II} = Ru: $[Ru(bpy)_2Cl_2]$ (1 equiv), EtOH, CH_2Cl_2, 90 °C, 3 days; (*iii*) KPF_6, DMF, H_2O.

In the past decade the interest in truxene chemistry has expanded, and it has been exploited mainly as a tunable highly fluorescent blue emitting material.[8−15] Among others, its extended aromatic structure is appealing for optoelectronic applications, like non-linear optics,[16,17] two-photon absorption,[18] and organic light-emitting diodes.[19] Few recent examples showed that truxene is a good energy donor partner if employed in supramolecular arrays like dyads[20] or rotaxanes[21] and that truxene derivatives can act as photoactive cores in star-shaped multichromophoric systems.[11,22]

We present here a newly designed series of arrays where terpyridine-Pt(II) acetylide and Ru(II) and Os(II) bipyridine complexes have been linked to a truxene platform. The choice of using a large aromatic unit to assemble polypyridine complexes of Pt(II), Ru(II), and Os(II), widely studied chromophores for the construction of antenna systems,[23] derives from the possibility of taking advantage of the peculiar three-dimensional topology and photophysical properties of the truxene scaffold. To the best of our knowledge there is only one case in which three π-conjugated terpyridine ligands have been linked to truxene in a symmetric fashion,[24] and few cases where truxene has been covalently linked to phosphorescent platinum(II) metal centers.[17,25] We are unaware about publications where bipyridine ligands were linked in an unsymmetric fashion opening the door to the preparation of multimetallic truxene based complexes in a controlled sequential protocol. The major challenge with truxene chemistry is to devise synthetic protocols able to reduce the C_3 symmetry and to step-by-step import three different modules. To the best of our knowledge such protocols are nonexistent, and no report on difunctionalization has been published so far. Here we fill the gap and disclose an original alternative to more classical symmetrical functionalizations.

The polypyridyl-Pt-acetylide motif is known for its interesting luminescence properties,[26−29] and has been recently recognized as an efficient generator of triplet states in appended aromatic chromophores; the spin−orbit coupling induced by the Pt heavy atom, in fact, leads to a rapid intersystem crossing in the appended chromophore, and triplet states otherwise difficult to observe in highly fluorescent molecules like perylenes or pyrenes become accessible.[30−32] Both singlet and triplet states of the truxene ligand can thus be involved in the photophysics of the arrays

(8) Kanibolotsky, A. L.; Berridge, R.; Skabara, P. J.; Perepichka, I. F.; Bradley, D. D. C.; Koeberg, M. *J. Am. Chem. Soc.* **2004**, *126*, 13695–13702.
(9) Zhang, W. B.; Jin, W. H.; Zhou, X. H.; Pei, J. *Tetrahedron* **2007**, *63*, 2907–2914.
(10) Luo, J.; Zhou, Y.; Niu, Z. Q.; Zhou, Q. F.; Ma, Y. G.; Pei, J. *J. Am. Chem. Soc.* **2007**, *129*, 11314–11315.
(11) Yuan, M. S.; Liu, Z. Q.; Fang, Q. *J. Org. Chem.* **2007**, *72*, 7915–7922.
(12) Pei, J.; Wang, J. L.; Cao, X. Y.; Zhou, X. H.; Zhang, W. B. *J. Am. Chem. Soc.* **2003**, *125*, 9944–9945.
(13) Wang, J. L.; Tang, Z. M.; Xiao, Q.; Zhou, Q. F.; Ma, Y. G.; Pei, J. *Org. Lett.* **2008**, *10*, 17–20.
(14) Cao, X. Y.; Zhang, W.; Zi, H.; Pei, J. *Org. Lett.* **2004**, *6*, 4845–4848.
(15) Oliva, M. M.; Casado, J.; Navarrete, J. T. L.; Berridge, R.; Skabara, P. J.; Kanibolotsky, A. L.; Perepichka, I. F. *J. Phys. Chem. B* **2007**, *111*, 4026–4035.
(16) Lambert, C.; Noll, G.; Schmalzlin, E.; Meerholz, K.; Brauchle, C. *Chem.—Eur. J.* **1998**, *4*, 2129–2135.
(17) Chan, C. K. M.; Tao, C. H.; Tam, H. L.; Zhu, N. Y.; Yam, V. W. W.; Cheah, K. W. *Inorg. Chem.* **2009**, *48*, 2855–2864.
(18) Zheng, Q. D.; He, G. S.; Prasad, P. N. *Chem. Mater.* **2005**, *17*, 6004–6011.
(19) Kimura, M.; Kuwano, S.; Sawaki, Y.; Fujikawa, H.; Noda, K.; Taga, Y.; Takagi, K. *J. Mater. Chem.* **2005**, *15*, 2393–2398.
(20) Sanchez, L.; Martin, N.; Gonzalez-Cantalapiedra, E.; Echavarren, A. M.; Rahman, G. M. A.; Guldi, D. M. *Org. Lett.* **2006**, *8*, 2451–2454.
(21) Wang, J. Y.; Han, J. M.; Yan, J.; Ma, Y. G.; Pei, J. *Chem.—Eur. J.* **2009**, *15*, 3585–3594.
(22) Diring, S.; Puntoriero, F.; Nastasi, F.; Campagna, S.; Ziessel, R. *J. Am. Chem. Soc.* **2009**, *131*, 6108–6110.
(23) Campagna, S.; Puntoriero, F.; Nastasi, F.; Bergamini, G.; Balzani, V. *Top. Curr. Chem.* **2007**, 280–281.
(24) Yuan, S. C.; Chen, H. B.; Zhang, Y.; Pei, J. *Org. Lett.* **2006**, *8*, 5701–5704.
(25) Diring, S.; Ziessel, R. *Tetrahedron Lett.* **2009**, *50*, 1203–1208.
(26) Wong, K. M. C.; Yam, V. W. W. *Coord. Chem. Rev.* **2007**, *251*, 2477–2488.
(27) Williams, J. A. G. *Top. Curr. Chem.* **2007**, *281*, 205–268.
(28) Wong, K. M. C.; Tang, W. S.; Chu, B. W. K.; Zhu, N. Y.; Yam, V. W. W. *Organometallics* **2004**, *23*, 3459–3465.
(29) Yang, Q. Z.; Wu, L. Z.; Wu, Z. X.; Zhang, L. P.; Tung, C. H. *Inorg. Chem.* **2002**, *41*, 5653–5655.
(30) Rachford, A. A.; Goeb, S.; Castellano, F. N. *J. Am. Chem. Soc.* **2008**, *130*, 2766–2767.
(31) Rachford, A. A.; Goeb, S.; Ziessel, R.; Castellano, F. N. *Inorg. Chem.* **2008**, *47*, 4348–4355.

Scheme 2. Synthesis of the **OsL**, **OsL_2**, **OsL_3**, **Ru−Os**, **Pt−Os**, and **Pt−Ru−Os** Complexes[a]

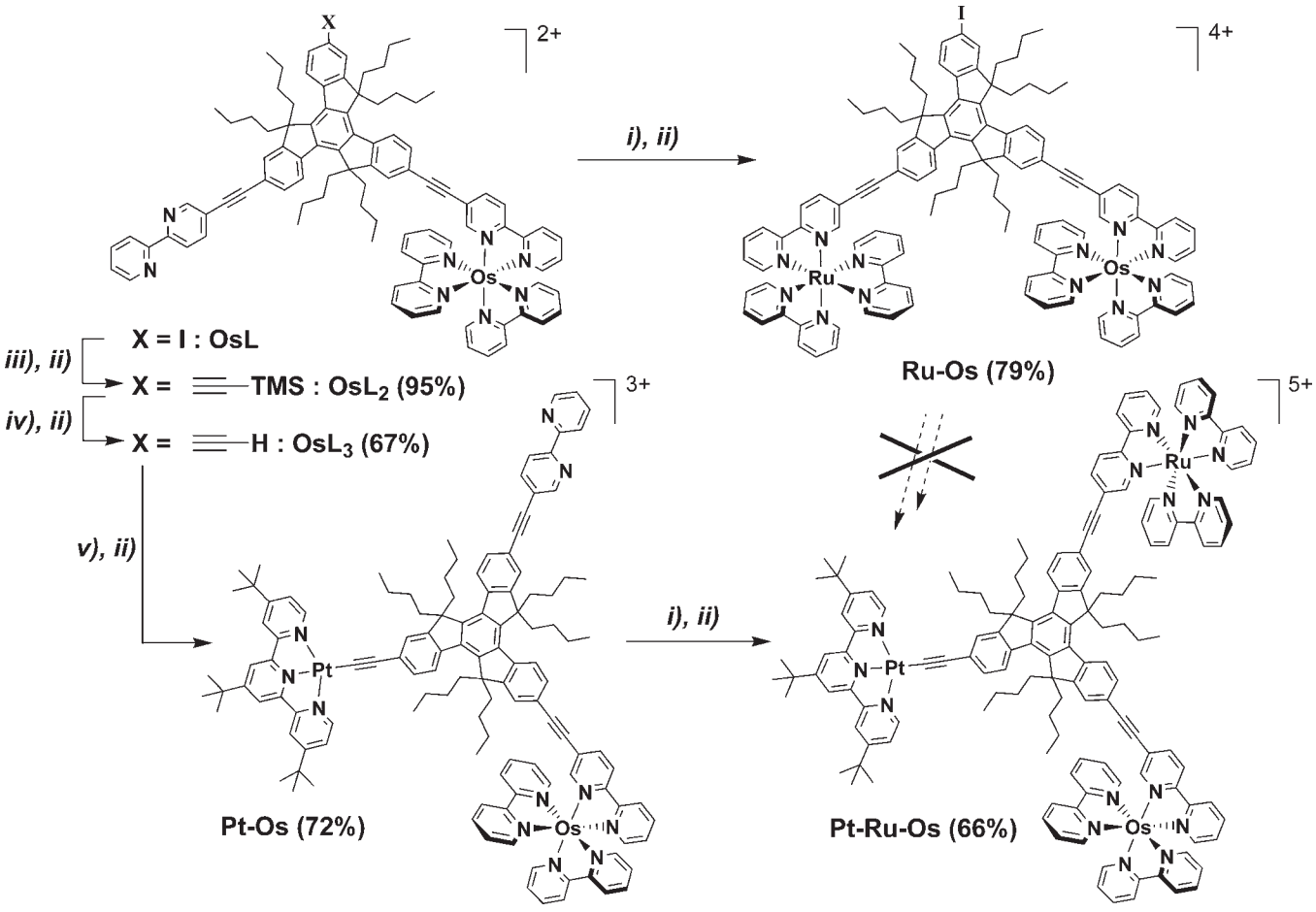

[a] (*i*) $[Ru(bpy)_2Cl_2]\cdot 6H_2O$, EtOH, CH_2Cl_2, 80 °C, 2-3 days; (*ii*) KPF_6, DMF, H_2O, RT; (*iii*) trimethylsilylacetylene, $[Pd(PPh_3)_4]$ (12%), diisopropylamine, CH_3CN, 65 °C, 18 h.; (*iv*) KF, EtOH, CH_2Cl_2, RT, 1 day; (*v*) [Pt (^{t}Bu$_3$tpy) Cl]BF_4, CuI (10%), Et_3N, CH_2Cl_2, RT, 3 days.

here presented; this study aims at understanding the role of the truxene core in the energy transfer dynamics of this new type of antenna systems.

The synthesis and a detailed photophysical characterization of a unique star-shaped trimetallic **Pt−Ru−Os** complex together with model mononuclear **PtL′**, **RuL**, and **OsL** complexes as well as dinuclear **Pt−Os** and **Ru−Os** complexes and ligands **L** and **L′** are herein presented (Schemes 1 and 2 and Chart 1). Simple mononuclear building blocks which lack the truxene fragment, **Pt**, **Ru**, and **Os** (Chart 1), are also reviewed for comparison purposes.

Experimental Section

Synthesis and Characterization. All reactions were performed under a dry atmosphere of argon using standard Schlenk tube techniques. All chemicals were used as received from commercial sources without further purification unless otherwise stated. CH_2Cl_2 and CH_3CN were distilled from P_2O_5 under an argon atmosphere. NEt_3 was allowed to stand over KOH pellets prior to use.

General Procedure for the Counterion Metathesis. The crude complex obtained after evaporation of the reaction mixture to dryness was dissolved in minimum amount of DMF (1 to 2 mL) and dropwise added through a Celite pad to a vigorously stirred aqueous solution of KPF_6 (1 g in 10 mL). The resulting precipitate was filtered off on paper and washed abundantly with distilled water until the filtrate was colorless. After drying, the complex was recovered and dissolved in dichloromethane. The resulting product was purified by column chromatography.

Ligand L. 2,7,12-Triiodo-5,5′-10,10′-15,15′-hexabutyltruxene (1.21 g, 1.15 mmol) and 5-ethynyl-2,2′-bipyridine (415 mg, 2.30 mmol) were dissolved in *n*-propylamine (40 mL). Argon was bubbled through the mixture for 30 min, then $[Pd(PPh_3)_4]$ (160 mg, 0.14 mmol) was added, and the mixture stirred at 60 °C for 18 h. After rotary evaporation of the solvent, the residue was extracted with dichloromethane and washed with water and saturated brine. The organic layer was filtered over hygroscopic cotton wool and evaporated. The target ligand was isolated from remaining starting material, monosubstituted and trisubstituted side products by column chromatography on aluminum oxide eluting with dichloromethane-petroleum ether (*v*/*v*: 1/9 to 3/7) to give 668 mg (50%) of **L** as yellowish white solid after recrystallization from dichloromethane-ethanol mixture; ^{1}H NMR ($(CD_3)_2CO$, 400 MHz): δ 8.89 (d, 2H, ^4J = 1.5 Hz), 8.72 (d, 2H, ^3J = 4.0 Hz), 8.60−8.52 (m, 6H), 8.33 (d, 1H, ^3J = 8.4 Hz), 8.13 (dd, 2H, ^3J = 8.2 Hz, ^4J = 2.0 Hz), 8.02 (d, 1H, ^4J = 1.8 Hz), 7.97 (td, 2H, ^3J = 7.7 Hz, ^4J = 1.7 Hz), 7.90−7.86 (m, 3H), 7.79−7.76 (m, 2H), 7.47−7.44 (m, 2H), 3.15−3.02 (m, 6H), 2.35−2.20 (m, 6H), 1.05−0.85 (m, 12H), 0.70−0.45 (m, 30H); ^{13}C NMR ($CDCl_3$, 75 MHz): δ 156.2, 153.9, 153.85, 146.5, 146.3, 145.6, 140.9, 140.8, 139.7, 139.5, 138.2, 138.1, 138.0, 137.3, 135.5, 131.7, 130.3, 126.6, 125.6, 124.8, 124.75, 120.6,

(32) Danilov, E. O.; Pomestchenko, I. E.; Kinayyigit, S.; Gentili, P. L.; Hissler, M.; Ziessel, R.; Castellano, F. N. *J. Phys. Chem. A* **2005**, *109*, 2465–2471.

Chart 1. Molecular Formulae of Ligands and Complexes Complementary to Schemes 1 and 2

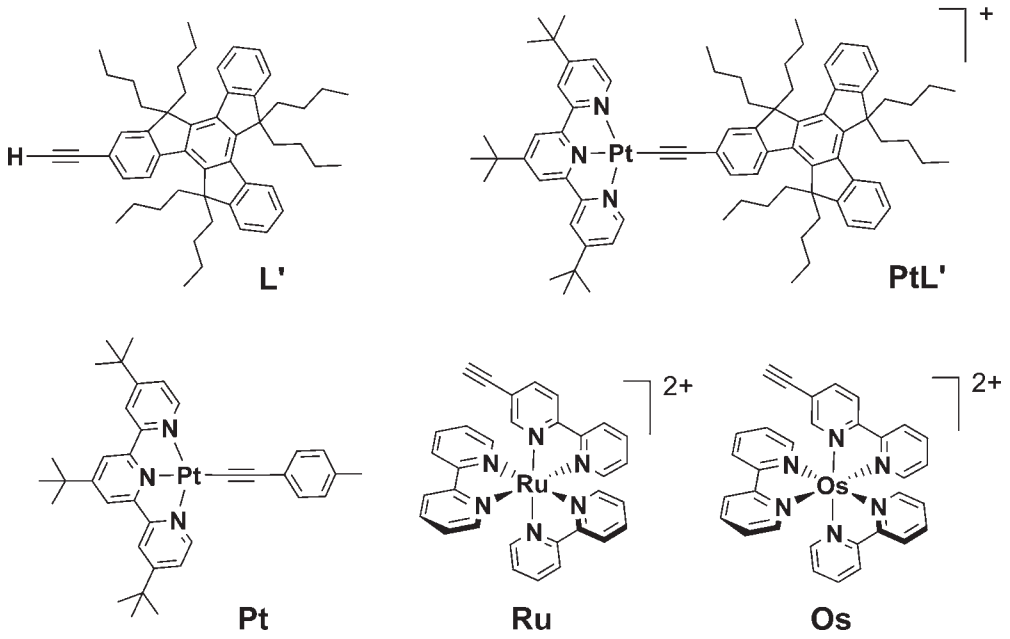

94.5, 92.8, 87.1, 56.1, 55.95, 55.9, 36.8, 36.7, 26.7, 26.6, 23.0, 22.95, 22.9, 14.0, 13.95, 13.9; EI-MS *m/e* (nature of the peak, relative intensity) 1161.2 ($[M]^+$, 100); Anal. Calcd. for $C_{75}H_{77}IN_4$: C, 77.57; H, 6.68; N, 4.82; Found: C, 77.38; H, 6.39; N, 4.67.

Complex OsL. Ligand **L** (345 mg, 0.30 mmol) and $[Os(bpy)_2Cl_2]$ (185 mg, 0.32 mmol) were suspended in ethyl alcohol (20 mL) in a Teflon reactor. The mixture was irradiated with microwaves (1200 W, 180 °C) for 1 h. The solvent was evaporated and counterion exchanged according to general procedure. After extraction with dichloromethane, the target compound was isolated from remaining starting material and bimetallic side product by column chromatography on aluminum oxide eluting with dichloromethane-methyl alcohol (*v*/*v*: 100/0 to 94/6) to afford 227 mg (40%) of **OsL** black crystals after recrystallization from dichloromethane-diethyl ether; ^{1}H NMR ($(CD_3)_2CO$, 400 MHz): δ 8.88−8.81 (m, 7H), 8.72 (d, 1H, 4.3 Hz), 8.58−8.51 (4H), 8.33−8.27 (m, 1H), 8.19−7.85 (m, 17H), 7.78−7.73 (m, 1H), 7.6−7.68 (m, 1H), 7.62−7.59 (m, 1H), 7.55−7.45 (m, 6H), 3.13−2.97 (m, 6H), 2.33−2.14 (m, 6H), 1.05−0.82 (m, 12H), 0.66−0.40 (m, 30H); ESI-MS *m/z* (nature of the peak, relative intensity) 1810.4 ($[M - PF_6]^+$, 100), 832.2 ($[M - 2PF_6]^{2+}$, 30); Anal. Calcd. for $C_{95}H_{93}F_{12}IN_8OsP_2$: C, 58.40; H, 4.80; N, 5.73; Found: C, 58.27; H, 4.59; N, 5.58.

Complex RuL. Ligand **L** (20 mg, 17 μmol) was dissolved in a mixture of ethyl alcohol (12 mL), and dichloromethane (2 mL). $[Ru(bpy)_2Cl_2]$ (8 mg, 17 μmol) was added, and the mixture was refluxed (90 °C) for 3 days. The solvent was then rotary evaporated. The counterion was exchanged as described in the general procedure, and the residue purified by column chromatography on aluminum oxide eluting with a mixture of dichloromethane and methyl alcohol (*v*/*v*: 100/0 to 94/6) to afford 16 mg (50%) of **RuL**; ^{1}H NMR ($(CD_3)_2CO$, 400 MHz): δ 8.92−8.82 (m, 7H), 8.75−8.70 (m, 1H), 8.58−8.50 (m, 4H), 8.40−8.21 (m, 9H), 8.15−7.95 (m, 6H), 7.91−7.84 (m, 2H), 7.78−7.73 (m, 1H), 7.69−7.59 (m, 7H), 7.49−7.42 (m, 2H), 3.15−2.95 (m, 6H), 2.33−2.13 (m, 6H), 1.03−0.83 (m, 12H), 0.67−0.40 (m, 30H). ESI-MS *m/z* (nature of the peak, relative intensity) 1719.4 ($[M - PF_6]^+$, 100), 787.3 ($[M - 2PF_6]^{2+}$, 30); Anal. Calcd. for $C_{95}H_{93}F_{12}IN_8RuP_2$: C, 61.19; H, 5.03; N, 6.01; Found: C, 60.95; H, 4.82; N, 5.79.

Complex Ru−Os. The target complex was prepared from **OsL** (50 mg, 25 μmol) and $[Ru(bpy)_2Cl_2]$, ethyl alcohol (30 mL), and dichloromethane (5 mL), and the mixture was heated at 80 °C for 3 days. Column chromatography on aluminum oxide eluting with dichloromethane-methyl alcohol (*v*/*v*: 98/2 to 95/5) to give 53 mg (79%) of **Ru−Os** as black crystals after recrystallization from dichloromethane-diethyl ether; ^{1}H NMR ($(CD_3)_2CO$, 400 MHz): δ 8.93−8.83 (m, 12H), 8.51 (d, 2H, ^3J = 8.4 Hz), 8.36 (dd, 1H, ^3J = 8.3 Hz, ^4J = 1.9 Hz), 8.28−7.93 (m, 25H), 7.85 (dd, 1H, ^3J = 8.5 Hz, ^4J = 1.7 Hz), 7.69−7.48 (m, 14H), 3.07−2.95 (m, 6H), 2.27−2.13 (m, 6H), 1.00−0.80 (m, 12H), 0.63−0.38 (m, 30H); ESI-MS *m/z* (nature of the peak, relative intensity) 1184.0 ($[M - 2PF_6]^{2+}$, 100), 741.4 ($[M - 3PF_6]^{3+}$, 30); Anal. Calcd. for $C_{115}H_{109}F_{24}IN_{12}OsP_4Ru$: C, 51.98; H, 4.13; N, 6.33; Found: C, 52.29; H, 4.40; N, 6.64.

Complex OsL_2. Complex **OsL** (168 mg, 86 μmol) was dissolved in acetonitrile (15 mL) and diisopropylamine (4 mL) in a Schlenk tube. Argon was bubbled through the mixture for 30 min, then $[Pd(PPh_3)_4]$ (12 mg, 10 μmol) and trimethylsilylacetylene (30 μL, 0.2 mmol) were added, and the mixture was stirred at 65 °C for 18 h. The solvent was then rotary evaporated, and the counterion was exchanged as described in the general procedure. After extraction with dichloromethane, the residue was purified by a quick column chromatography on silica gel eluting with dichloromethane-methyl alcohol (*v*/*v*: 95/5) to give 157 mg (95%) of **OsL_2** as black crystals after recrystallization from dichloromethane-diethylether; ^{1}H NMR ($(CD_3)_2CO$, 400 MHz): δ 8.89−8.81 (m, 6H), 8.72 (m, 1H), 8.59−8.45 (m, 5H), 8.19−7.94 (m, 14H), 7.86 (dd, 1H, ^3J = 8.6 Hz, ^4J = 1.6 Hz), 7.79−7.44 (m, 12H), 3.13−2.98 (m, 6H), 2.33−2.15 (m, 6H), 1.03−0.82 (m, 12H), 0.65−0.40 (m, 30H), 0.29 (s, 9H); ESI-MS *m/z* (nature of the peak, relative intensity) 1779.5 ($[M - PF_6]^+$, 100), 817.3 ($[M - 2PF_6]^{2+}$, 35); Anal. Calcd. for $C_{100}H_{102}F_{12}N_8OsP_2Si$: C, 62.42; H, 5.34; N, 5.82; Found: C, 62.59; H, 5.08; N, 5.62.

Complex OsL_3. KF (10 mg, 172 μmol) and complex **OsL_2** (33 mg, 17 μmol) were dissolved in a mixture of ethyl alcohol (10 mL), dichloromethane (1 mL), and water (0.2 mL) and stirred in the dark at room temperature (RT) for 24 h. The solvent was evaporated, and the counterion was exchanged as described in the general procedure After dichloromethane extraction the residue was quickly filtered over aluminum oxide eluting with dichloromethane-methyl alcohol (96/4) to give 21 mg (67%) of **OsL_3** as a dark solid; ^{1}H NMR ($(CD_3)_2CO$, 400 MHz): δ 8.89−8.81 (m, 6H), 8.72 (d, 1H, ^3J = 4.0 Hz), 8.59−8.46 (m, 5H), 8.20−7.94 (m, 14H), 7.87 (dd, 1H, ^3J = 9.5 Hz, ^4J = 1.5 Hz),

7.79−7.45 (m, 12H), 3.78 (d, 1H, J = 1.5 Hz), 3.14−2.98 (m, 6H), 3.24−2.15 (m, 6H), 1.03−0.83 (m, 12H), 0.68−0.38 (m, 30H); ESI-MS m/z (nature of the peak, relative intensity) 1709.2 ($[M - PF_6]^+$, 100), 782.0 ($[M - 2PF_6]^{2+}$, 15); Anal. Calcd. for $C_{97}H_{94}F_{12}N_8OsP_2$: C, 62.91; H, 5.12; N, 6.05; Found: C, 63.27; H, 5.54; N, 6.39.

Complex Pt−Os. Complex $\mathbf{OsL_3}$ (20 mg, 10.7 μmol) and [Pt(^{t}Bu$_3$tpy)Cl]BF_4 (12 mg, 16.7 μmol) were dissolved in dichloromethane (6 mL). Triethylamine (2 mL) was added and argon was bubbled through the mixture for 30 min, after which CuI (0.2 mg, 1 μmol) was added, and the reaction mixture was stirred in the dark at RT for 3 days. The counterion was exchanged as described in the general procedure. The residue was treated with water and extracted with dichloromethane. The organic extracts were washed with water and filtered through hygroscopic cotton wool. The solvent was removed by rotary evaporation, and the residue was purified by column chromatography on silica gel eluting with dichloromethane−methyl alcohol (v/v: 99.5/0.5 to 94/6) to give 20 mg (72%) of **Pt−Os** as black crystals after recrystallization from acetone-diethyl ether; ^{1}H NMR ($(CD_3)_2CO$, 400 MHz): δ 9.34 (d, 2H, ^3J = 5.5 Hz), 8.87−8.77 (m, 12H), 8.60−8.44 (m, 5H), 8.19−7.86 (m, 17H), 7.77−7.67 (m, 4H), 7.63−7.60 (m, 1H), 7.56−7.48 (m, 6H), 3.18−3.00 (m, 6H), 2.37−2.18 (m, 6H), 1.56 (s, 9H), 1.52 (s, 18H), 1.05−0.87 (m, 12H), 0.73−0.45 (m, 30H); ESI-MS m/z (nature of the peak, relative intensity) 2448.0 ($[M - PF_6]^+$, 100), 1151.4 ($[M - 2PF_6]^{2+}$, 45), 719.0 ($[M - 3PF_6]^{3+}$, 25); Anal. Calcd. for $C_{124}H_{128}F_{18}N_{11}OsP_3Pt$: C, 57.44; H, 4.98; N, 5.94; Found: C, 57.62; H, 5.17; N, 6.17.

Complex Pt−Ru−Os. This complex was prepared from **Pt−Os** (17 mg, 6.5 μmol), [Ru(bpy)$_2$Cl$_2$] (4.1 mg, 7.8 μmol), ethyl alcohol (6 mL), and dichloromethane (1 mL), and the mixture was heated at 80 °C for 2 days. The counterion was exchanged as described in the general procedure. Column chromatography on silica gel eluting with dichloromethane-methyl alcohol (v/v: 99/1 to 94/6) afforded 14 mg (66%) of **Pt−Ru−Os** as black crystals after recrystallization from acetone - diethyl ether; ^{1}H NMR ($(CD_3)_2CO$, 400 MHz): δ 9.34 (d, 2H, ^3J = 6.0 Hz), 8.91−8.79 (m, 16H), 8.54 (t, 2H, ^3J = 8.6 Hz), 8.43 (d, 1H, ^3J = 8.0 Hz), 8.38−8.35 (m, 1H), 8.27−7.94 (m, 25H), 7.71−7.49 (m, 16H), 3.16−2.99 (m, 6H), 2.30−2.14 (m, 6H), 1.55 (s, 9H), 1.51 (s, 18H), 1.04−0.83 (m, 12H), 0.72−0.41 (m, 30H); ESI-MS m/z (nature of the peak, relative intensity) 3151.0 ($[M - PF_6]^+$, 25), 1503.4 ($[M - 2PF_6]^{2+}$, 100), 953.3 ($[M - 3PF_6]^{3+}$, 15); Anal. Calcd. for $C_{144}H_{144}F_{30}N_{15}OsP_5PtRu$: C, 52.47; H, 4.40; N, 6.37; Found: C, 52.64; H, 4.57; N, 6.50.

General Instrumentation. ^{1}H NMR (400.1 MHz) spectra were recorded at RT on a Bruker Avance 400 MHz spectrometer using perdeuterated solvents as internal standards (δ d_6-acetone 2.04 ppm). Chromatographic purifications were performed using deactivated alumina (including 6% water by weight). TLC was performed on silica gel or alumina plates coated with fluorescent indicator. Mass spectra were measured with a JEOL JMS-T100 LO Acc TOF (ESI-MS). Elemental analysis was conducted by an Elementar vario MICRO Cube.

Photophysical Measurements. Spectroscopic grade solvents (C. Erba) were used as received. The absorption spectra of dilute solutions (10^{-6} M) were recorded on a Perkin-Elmer Lambda 950 UV/vis/NIR spectrophotometer in 1 cm path length optical Suprasil Quartz (QS) cells.

Emission spectra were measured in right angle mode using a Spex Fluorolog II spectrofluorimeter, equipped with a Hamamatsu R928 phototube. Corrected spectra were employed throughout this work by applying to the raw data a correction curve for the wavelength dependent phototube response between 280 and 900 nm obtained by using a calibrated halogen lamp source. Air-free samples were obtained by bubbling the solutions for 10 min with a stream of argon in home modified 1 cm fluorescence cells. Luminescence quantum yields (ϕ_{em}) were evaluated from the area of the luminescence spectra, corrected for the photomultiplier response, with reference to quinine sulfate in air-equilibrated 1 N H_2SO_4 (ϕ_r = 0.546)[33] for the ligands and to [Ru(bpy)$_3$]Cl$_2$ in air-equilibrated water (ϕ_r = 0.028)[33] for the complexes, by using the following equation:[34]

$$\phi_{em} = \frac{A_r n^2 I}{n_r^2 I_r A}\phi_r$$

where A and n are the absorbance values at the employed excitation wavelength and refractive index of the solvent, respectively. The concentration of the sample solutions was adjusted to obtain absorption values $A < 0.15$ at the excitation wavelength. Estimated uncertainties on band maxima and luminescence intensities are 2 nm and 20%, respectively. Experiments at 77 K in MeOH/EtOH (1:4) frozen glasses made use of quartz capillary tubes immersed in liquid nitrogen contained in a homemade quartz dewar. Excitation spectra, both at RT and at 77 K, were obtained at the different luminescence peaks, by using the same Spex Fluorolog II spectrofluorimeter. Luminescence lifetimes in the ns-μs range were measured with an IBH 5000F time-correlated single-photon counting device, by using pulsed NanoLED excitation sources at 278 nm, 331 nm, 465 nm, and 560 nm (pulse width ≤0.6 ns). Analysis of the luminescence decay profiles against time was accomplished with the DAS6 Decay Analysis Software provided by the manufacturer. Experimental uncertainties in the lifetime determinations are estimated to be 10%.

Phosphorescence spectra and decays in the ms-s range were measured at 77 K in MeOH/EtOH (1:4) frozen dilute solutions on a Perkin-Elmer LS-50B spectrofluorimeter equipped with a pulsed Xe lamp and in gated detection mode. The phosphorescence decay analysis was performed with the PHOSDecay software provided by the manufacturer.

Transient absorbance in the nanosecond range made use of a laser flash photolysis apparatus based on a Nd:YAG laser (JK Lasers) delivering pulses of 18 ns.[35] The third harmonic (266 nm) was used for excitation. The pulse energy used was 1.0 mJ/pulse for the determination of the spectra and of the order of 0.2 mJ/pulse for the triplet lifetimes determination. The concentration of the solutions of the single components was adjusted to absorb the same number of photons absorbed by the corresponding units in the **PtL′** solution (A = 0.9 at 266 nm). Experiments were conducted in homemade, 1 cm optical path cuvettes; the solutions were bubbled with argon for 10 min to remove dissolved oxygen and sealed. The working temperature, if not otherwise specified, was 295 ± 2 K.

All the examined compounds were found to be thermally and photochemically stable in solution, with the exception of a moderate photolability of the two ligands **L** and **L′** under laser irradiation.

Results and Discussion

Synthesis. The most reliable synthetic strategy adopted to connect the three distinct metal fragments to the truxene core employs 2,7,12-triiodo-5,5′,10,10′,15,15′-hexabutyltruxene as starting material. Initially, selective introduction of two 5-ethynyl-2,2′-bipyridine fragments leading to ligand **L** could be achieved via a Pd(0) promoted statistical cross coupling reaction (Scheme 1). The first metal being complexed to **L** is the Os(II) cation using a microwave assisted heating with [Os(bpy)$_2$Cl$_2$] as metal precursor. After counteranion exchange and chromatography

(33) Montalti, M.; Credi, A.; Prodi, L.; Gandolfi, M. T. *Handbook of Photochemistry*, 3rd ed.; CRC Press, Taylor & Francis: Boca Raton, FL, 2006.
(34) Demas, J. N.; Crosby, G. A. *J. Phys. Chem.* **1971**, *75*, 991–1024.
(35) Flamigni, L. *J. Phys. Chem.* **1992**, *96*, 3331–3337.

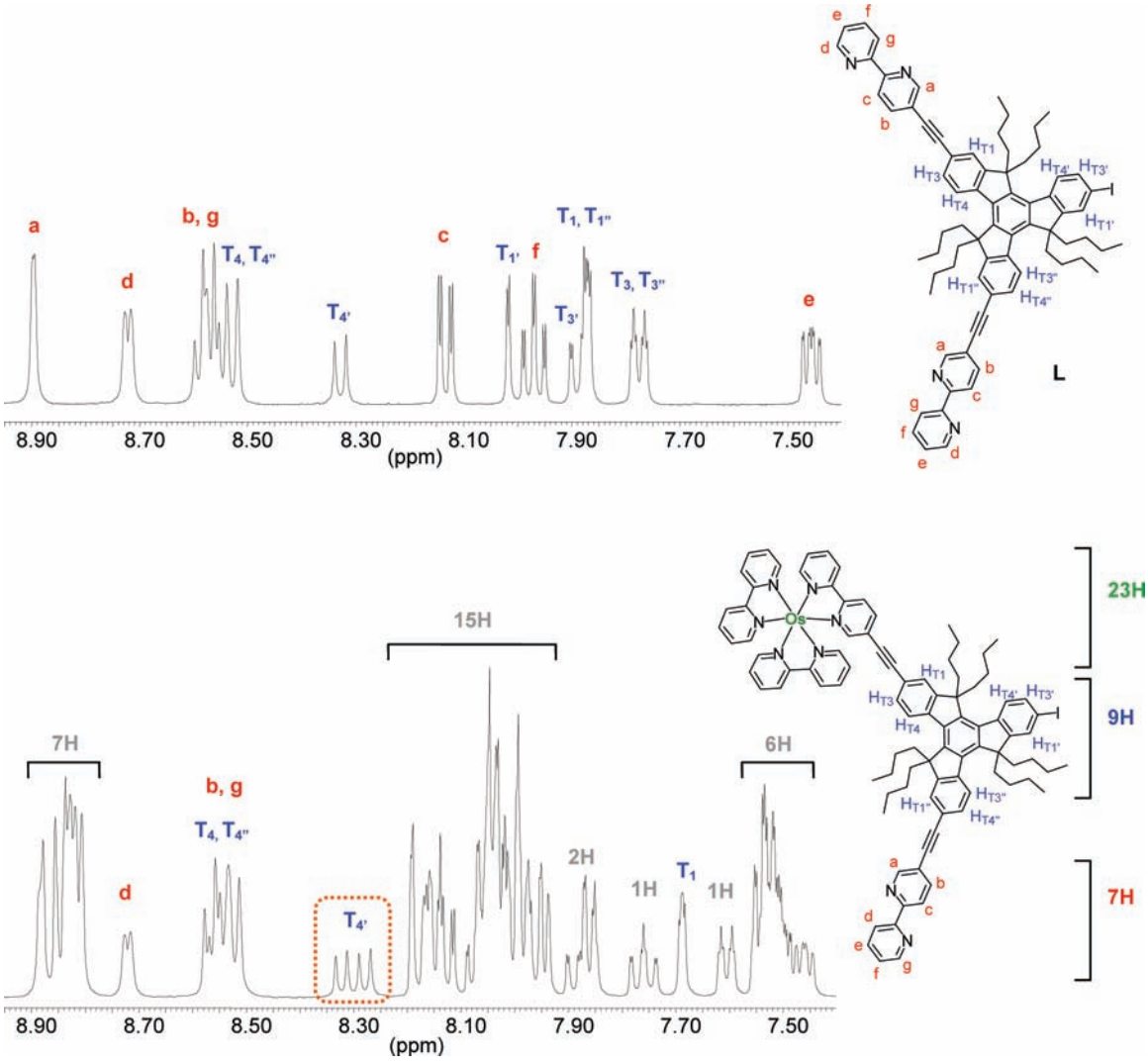

Figure 1. ^{1}H NMR spectra of compounds **L** (top), and **OsL** (bottom) in d_6-acetone, 400 MHz (for the sake of clarity only the aromatic regions are represented). The integration of each pattern is also given.

purification, the **OsL** complex was isolated in reasonable yield (40%). Likewise **RuL** (Scheme 1) and **Ru**−**Os** (Scheme 2) were prepared using a conventional protocol. Meanwhile, an acetylenic functionality was introduced on complex **OsL** via a Sonogashira[36] cross-coupling reaction with trimethylsilylacetylene affording complex $\mathbf{OsL_2}$ in almost quantitative yield (Scheme 2). Ensuing deprotection using potassium fluoride afforded the terminal alkyne derivative $\mathbf{OsL_3}$. A Cu(I) catalyzed coupling reaction with $[Pt(^tBu_3tpy)Cl]^+$ led to the **Pt**−**Os** complex. The target triad **Pt**−**Ru**−**Os** was obtained by complexation of the remaining bipyridine by reaction with $[Ru(bpy)_2Cl_2]\cdot 2H_2O$ under standard conditions (Scheme 2). Worth noting is the fact that the choice of another complexation sequence failed because of the stereoelectronic complexation demands requested by the Pt center. Other reference compounds are prepared using previously reported procedures (Chart 1).

All compounds were characterized by ^{1}H NMR spectroscopy, mass spectrometry, and elemental analysis. The solubility gained from the six butyl chains grafted on the truxene core as well as the hexafluorophosphate counterions allowed to record well-defined ^{1}H NMR spectra even for the trimetallic complex excluding the presence of aggregates (Figures 1 and 2).

Attribution of the NMR peaks was possible with the help of 2D COSY NMR sequence and provides a clear picture of the peak attribution in the free ligand **L**, which is very helpful to understand the NMR patterns of the complexes (Figure 1). In the case of **OsL** the doublet at 8.72 ppm with an integration of one proton confirms the presence of an uncoordinated bipyridine fragment. Particularly informative is the presence of two doublets at 8.30 ppm integration for one proton for the H_{T4}' localized in β-position of the iodo atom. This observation confirms the presence of two regio-isomers in a one-to-one ratio as would be expected from a C_3 symmetry and the presence of three five-member ring in the central position. All additional patterns and integrations match the expected one for complexation of a single bipyridine with an osmium center.

The **Ru**−**Os** dyad presents many complex aromatic signals because of the numerous coordinated 2,2′-bipyridine

(36) Sonogashira, K. *Comprehensive Organic Synthesis*; Pergamon Press: Oxford, 1990; Vol. *3*, pp 545−547.

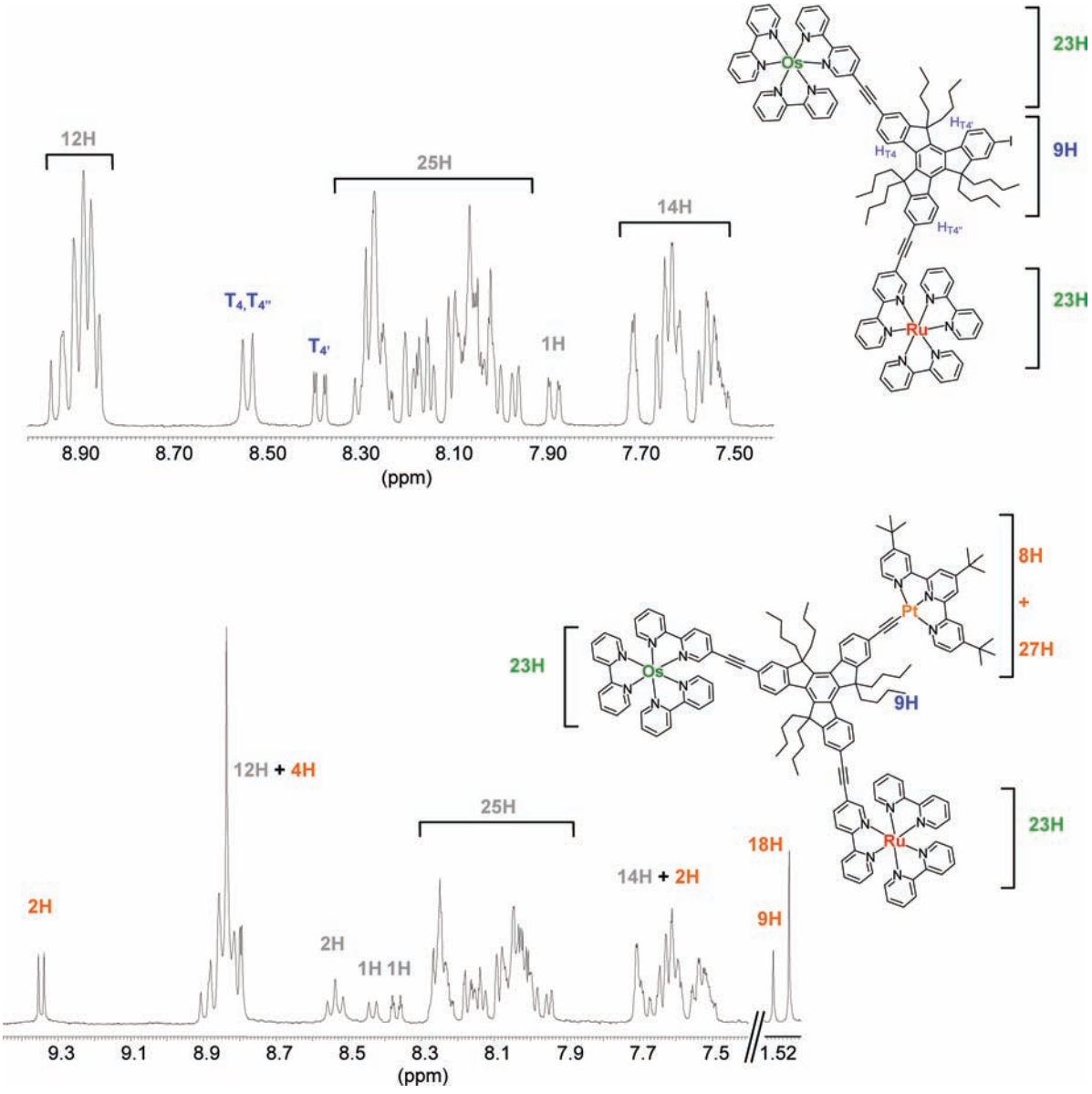

Figure 2. ^{1}H NMR spectra for complexes **Ru**−**Os** (top) and **Pt**−**Ru**−**Os** (bottom), in d_6-acetone, 400 MHz (for sake of clarity only the aromatic regions are represented). The integration of each pattern is also given.

residues around the truxene platform (Figure 2). Integration, however, confirmed the number of expected aromatic protons. Moreover, two signals (8.51 ppm, doublet, 2H, ^{3}J = 8.4 Hz) and 8.36 ppm (doublet of doublet, 1H, ^{3}J = 8.3 Hz, ^{4}J = 1.9 Hz) are safely assigned to protons H_{T4}-$H_{T4"}$ and H_{T4}' respectively, located on the aromatic periphery of the truxene moiety (based on NMR experiments performed on **L** and **OsL**, see Figure 1).

The single doublet at 8.51 ppm with a 2 proton integration, arising from H_{T4}-$H_{T4"}$ protons indicates that the octahedral Ru(II) and Os(II) fragments are producing very close magnetic environments. The presence of Pt(II)-acetylide fragment in **Pt**−**Ru**−**Os** is confirmed by the integration of eight supplementary protons in the aromatic region. A characteristic doublet at 9.34 ppm (^{3}J = 6.0 Hz) with underlying ^{195}Pt satellites is attributed to the protons located in α position to the external pyridine nitrogen atoms of the terpyridine fragment. Furthermore, in the aliphatic region two singlets at 1.55 ppm (9H) and 1.51 ppm (18H) account for the 27 protons of the *tert*-butyl group on the terpyridine periphery.

Optical Absorption. The absorption data are listed in Table 1. Figure 3 shows the absorption spectra of the mononuclear complexes **PtL′**, **RuL**, and **OsL** compared with those of precursors **Pt**, **Ru**, and **Os** and ligands **L′** and **L**. The sum of the spectra of the respective simpler precursor and the corresponding truxene ligand is also reported for each complex in the graphs. Ligand **L′** shows absorption bands of $^{1}\pi,\pi^*$ nature below 350 nm peaking at 308 nm (ε = 75,300 M^{-1} cm^{-1}, Table 1), in agreement with literature data on simple truxene and ethynyl derivatives.[22,25,37] Ligand **L** shows an absorption spectrum localized below 400 nm with maximum at 352 nm (ε = 104,900 M^{-1} cm^{-1}, Table 1) that can be attributed to

(37) Perez, E. M.; Sierra, M.; Sanchez, L.; Torres, M. R.; Viruela, R.; Viruela, P. M.; Orti, E.; Martin, N. *Angew. Chem., Int. Ed.* **2007**, *46*, 1847–1851.

Table 1. Absorption Properties of the Examined Compounds[a]

	λ_{max} (nm)	ε ($M^{-1}\cdot cm^{-1}$)
L′	284	42,800
	308	75,300
	325	40,200
L	240	44,200
	352	104,900
	373	95,300
Pt	280	34,600
	327	18,900
	440	2,600
PtL′	285	73,200
	308	92,600
	333	81,600
	470	9,400
Ru[b]	288	70,000
	452	11,240
RuL	288	113,700
	319	98,300
	348	84,700
	367	83,600
	450	13,800
Os[b]	291	77,200
	449	11,900
	482	11,000
	580	3,900
OsL	291	112,500
	319	93,800
	347	83,800
	367	82,100
	480	11,600
	600	3,300
Pt−Os	242	100,000
	291	141,500
	336	154,400
	470	22,100
	600	3,600
Ru−Os	239	68,700
	290	166,600
	316	110,000
	386	84,300
	470	22,000
	600	3,300
Pt−Ru−Os	241	107,300
	289	192,200
	329	138,100
	386	100,000
	470	30,700
	600	3,400

[a] In air-equilibrated solvents, CH_2Cl_2 for **L** and **L′** and CH_3CN for the complexes, at 298 K. [b] From ref 40.

$^1\pi,\pi^*$ transitions of the truxene core, red-shifted and less structured with respect to that of unsubstituted truxene because of the increased conjugation brought about by the acetylene linked bipyridine groups.[6,12,14,15,24] The models **Pt**, **Ru**, and **Os** display typical terpy or bpy centered $^1\pi,\pi^*$ absorption below 300 nm and ^{1}MLCT transitions in the range 350−550 nm, with the addition, for **Os**, of an absorption tail peaking at 600 nm that has to be ascribed to formally forbidden ^{3}MLCT transitions;[38] a more detailed analysis of the absorption properties of these complexes can be found in our previous work.[39−41] Comparison of the spectra of complexes **PtL′**, **RuL**, and **OsL** with the sum of the spectra of their model components, that is, the corresponding metal precursor and ligand (Figure 3), shows some discrepancies: **PtL′** has a more intense and red-shifted CT absorption in the region 400−500 nm with respect to its precursor **Pt** (Figure 3a), probably because of the presence of both Pt→terpy and Pt→truxene transitions in **PtL′**; also the presence of C≡C→truxene ILCT transitions cannot be excluded.[17]

For **RuL** and **OsL**, instead, an evident decrease in the absorption intensity by the truxene ligand at 340−370 nm is accompanied by the appearance of a shoulder in the region 400−450 nm (Figure 3b−c). This is ascribable to the different electronic conditions experienced by ligand **L** when attached to the metal center, the MLCT transition

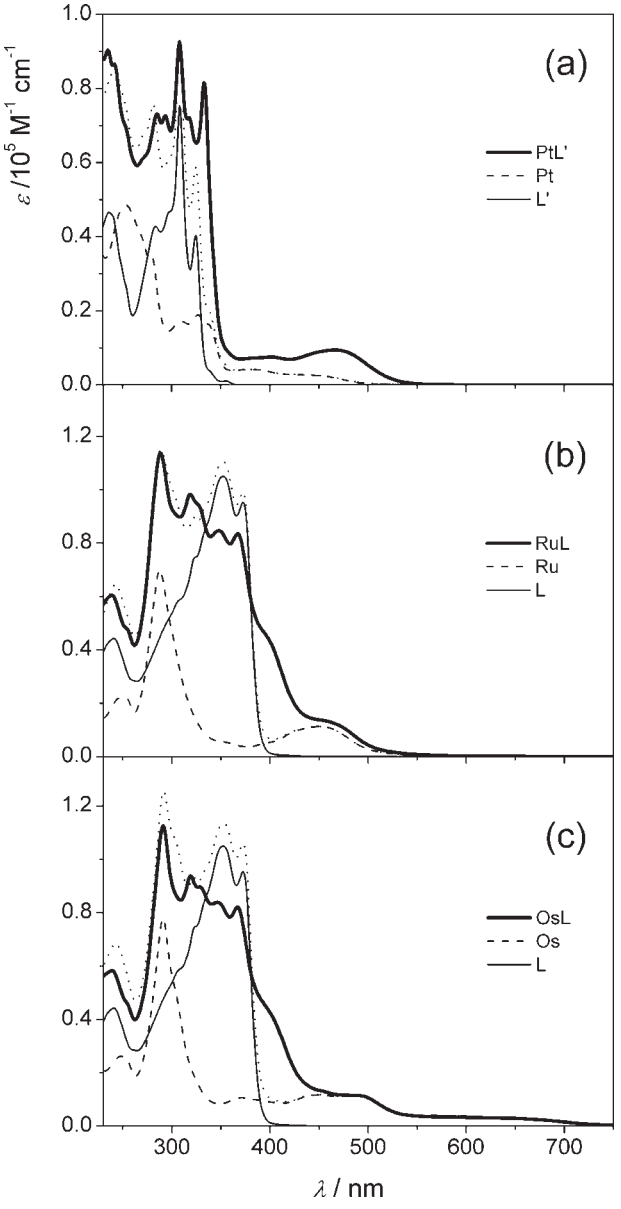

Figure 3. Absorption spectra of CH_3CN solutions of (a) **PtL′**, (b) **RuL**, and (c) **OsL** compared with those of the respective precursors **Pt**, **Ru**, and **Os** and ligands **L′** and **L** (in CH_2Cl_2 solutions). The sum of the spectra of the respective precursor and ligand is also reported in each graph as a dotted line.

(38) Kumaresan, D.; Shankar, K.; Vaidya, S.; Schmehl, R. H. Photochemistry and photophysics of coordination compounds: Osmium. In *Photochemistry and Photophysics of Coordination Compounds II*; Balzani, V., Campagna, S., Eds.; Springer-Verlag: Berlin, 2007; Vol. *281*, pp 101−142.
(39) Ventura, B.; Barbieri, A.; Zanelli, A.; Barigelletti, F.; Seneclauze, J. B.; Diring, S.; Ziessel, R. *Inorg. Chem.* **2009**, *48*, 6409–6416.
(40) Ventura, B.; Barbieri, A.; Barigelletti, F.; Seneclauze, J. B.; Retailleau, P.; Ziessel, R. *Inorg. Chem.* **2008**, *47*, 7048–7058.
(41) Ziessel, R.; Seneclauze, J. B.; Ventura, B.; Barbieri, A.; Barigelletti, F. *Dalton Trans.* **2008**, 1686–1688.

at low energy being unaffected. It can be concluded, thus, that electronic interactions between the metal complexes and the truxene ligands occur in all the examined complexes, but while the MLCT excited states of complexes **RuL** and **OsL** are considerably unaffected by the presence of the ligand, those of **PtL′** are markedly influenced, as confirmed also by the luminescence properties of this complex described in the relevant section. To get more insights into the nature of the excited states of **PtL′** a spectroscopic characterization of both **Pt** and **PtL′** in CH_2Cl_2 was also performed and is reported in the Supporting Information. Figure 4 shows the absorption spectra in CH_3CN of the multichromophoric arrays, that is, dyads **Pt−Os**, **Ru−Os**, and triad **Pt−Ru−Os**. It is interesting to note that in these systems the absorption spectrum of each array reasonably matches the sum of the absorption spectra of the respective components **PtL′**, **RuL**, and **OsL**, not reported in the figure for simplicity, after the ligand contribution is properly subtracted from the sums. This means that the Pt, Ru, and Os subunits of **PtL′**, **RuL**, and **OsL**, respectively, can be regarded as only weakly interacting with the other components in the dyads and in the triad, and thus represent good models for the photophysical characterization of the metal based excited states dynamics in the arrays. Since truxene excited states have an important role in the photophysics of **Pt−Os**, **Ru−Os**, and **Pt−Ru−Os**, this aspect will be examined in detail in the discussion below.

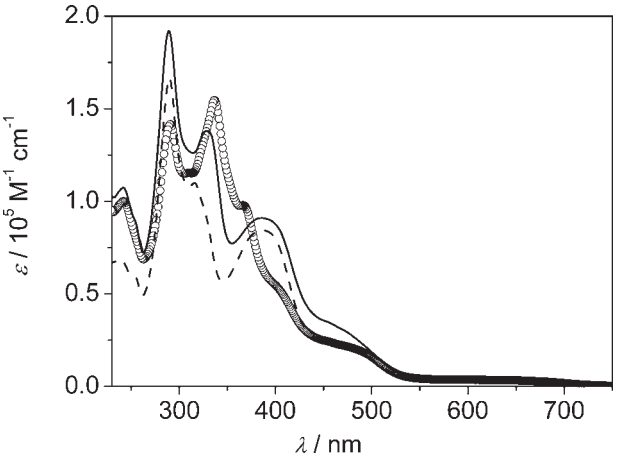

Figure 4. Absorption spectra of CH_3CN solutions of dyads **Pt−Os** (open circles), **Ru−Os** (dashed line), and triad **Pt−Ru−Os** (full line).

Luminescence of Truxene Ligands. The luminescence properties of ligands **L′** and **L** are summarized in Table 2, and Figure 5 compares their emission features. Ligand **L′** shows a structured emission with maxima at 358 and 375 nm, $\phi_{em} = 0.40$, and $\tau = 34.6$ ns at RT in degassed CH_2Cl_2. At low temperature the same structured fluorescence is observed, slightly blue-shifted with respect to the RT case (Table 2 and Figure 5a). Ligand **L** shows an intense structureless RT emission that peaks at 408 nm with a significantly higher emission quantum yield, $\phi_{em} = 0.70$, and $\tau = 0.86$ ns in degassed CH_2Cl_2 (Table 2 and Figure 5b). The red-shift of the **L** emission with respect to that of **L′** is attributed to the electronic delocalization induced in the truxene core by the acetylene-linked bipyridine groups, an effect already observed for conjugated truxene derivatives.[14,24] It is interesting to note that the lifetime of **L** fluorescence is greatly shortened with respect to that of **L′** and is accompanied by a substantial increase in the emission quantum yield (Table 2), resulting in a high k_r value of 8×10^8 s^{-1}; $k_r = \phi_{em}/\tau$.

In glassy matrix at 77 K, ligand **L** shows a structured fluorescence that peaks at 382 nm. Interestingly, both **L′** and **L** show phosphorescence in frozen solvent at 77 K (Table 2 and Figure 5). In both cases the phosphorescence spectrum exhibits the vibronic shape of the low temperature fluorescence; from the phosphorescence peak, the evaluated energy content of the lowest triplet excited state of **L′** and **L** is 2.58 and 2.29 eV, respectively. The measured phosphorescence lifetimes are 4.3 s and 17.5 ms for **L′** and **L**, respectively: **L′** phosphorescence has the same order of magnitude of that of basic truxene, for which a value of 13.3 s is reported in a previous study,[42] whereas **L** phosphorescence is much

Table 2. Luminescence Data for the Examined Compounds[a]

		298 K			77 K		
		λ_{max} (nm) [b]	ϕ_{em} [c]	τ (ns) [d]	λ_{max} (nm) [b]	τ (μs) [d]	E (eV)
L′	^{1}L′	358, 375	0.40	34.6	352, 372, 389	54.6×10^{-3}	3.52
	^{3}L				480, 519, 558	4.3×10^6	2.58
L	^{1}L	408	0.70	0.86	382, 404	0.71×10^{-3}	3.25
	^{3}L				542, 579	17.5×10^3	2.29
Pt	^{3}Pt	622	0.013	310.0	523	20.0	2.37
PtL′	^{3}Pt	674	2.8×10^{-3}	22.0	550	8.7	2.27
	^{3}L′				496, 529	5.8×10^6	2.50
Ru[e]	^{3}Ru	652	0.054	800.0	619	4.6	2.02
RuL	^{3}Ru	655	0.073	1040.0	614	4.5	2.02
Os[e]	^{3}Os	798	7.6×10^{-4}	16.0	736	2.3	1.68
OsL	^{3}Os	801	1.1×10^{-3}	22.2	744	0.84	1.67
Pt−Os	^{3}Os	802	1.1×10^{-3}	20.0	740	0.79	1.68
	^{3}L				530, 569	n.d.	2.33
Ru−Os	^{3}Ru	655	5.9×10^{-4}	2.3	616	n.d.	2.01
	^{3}Os	805	1.0×10^{-3}	−2.5, 22.6	746	0.82	1.66
Pt−Ru−Os	^{3}Ru	655	5.9×10^{-4}	2.5	613	n.d.	2.03
	^{3}Os	800	9.7×10^{-4}	21.3[f]	740	0.75	1.68

[a] In air-free solvents, CH_2Cl_2 for the ligands and CH_3CN for the complexes, at 298 K. In MeOH/EtOH (1:4 v/v) at 77 K. [b] Values from corrected emission spectra. [c] $\lambda_{exc} = 350$ nm for **L**, 470 nm for Pt- and Ru-based emission and 600 nm for Os-based emission. [d] $\lambda_{exc} = 331$ nm for **L**, 278 nm for **L′**, 465 nm for Pt- and Ru-based emission and 560 nm for Os-based emission. [e] From ref 40 and partially revised. [f] Not possible to fit the rise.

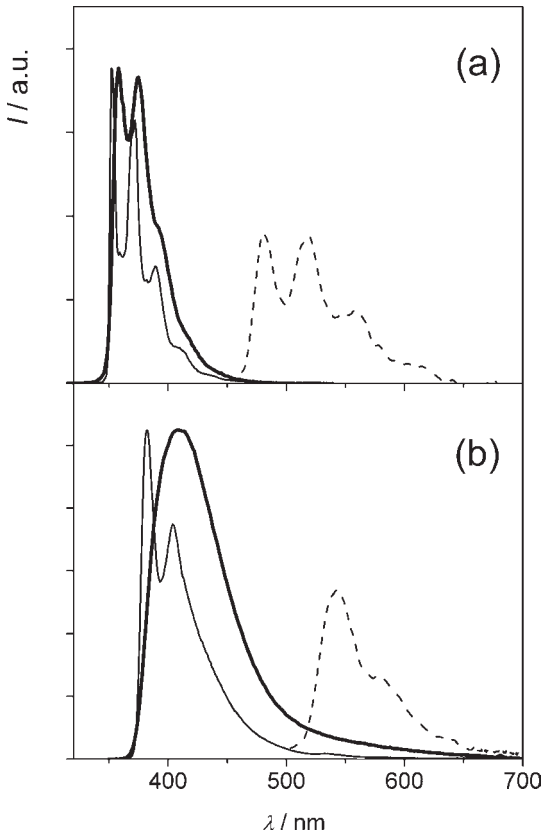

Figure 5. Arbitrarily scaled non-corrected emission spectra of (a) **L′** and (b) **L**. The graphs show: RT emission spectra in CH_2Cl_2 solution (thick), fluorescence (thin), and phosphorescence (dashed) spectra at 77 K in MeOH:EtOH (1:4 v/v). Excitation at 285 nm for **L′** and at 340 nm for **L**.

shorter-lived, probably because of the heavy atom effect of iodine that promotes the $T \rightarrow S_0$ spin forbidden deactivation.

Luminescence of Pt Model Complex. As commented above for the absorption data, complex **PtL′** behaves quite differently from its precursor **Pt**, and this is confirmed by luminescence: the **PtL′** emission shows a lower quantum yield (0.0028 vs 0.013) and a much shorter lifetime (22 ns vs 310 ns) with respect to **Pt** (Table 2). The characterization of **Pt** and **PtL′** in CH_2Cl_2, (see Supporting Information, Table S1 and Figure S1) confirms the poorer emission properties of **PtL′** with respect to **Pt**. This feature can be attributed to a somewhat different nature of the emitting state in **PtL′** with respect to **Pt**, since the presence of a mixed MLCT/ILCT state has been proposed in the former on the basis of the absorption data. The emission spectrum of **PtL′** upon excitation at 450 nm in glassy solvent at 77 K shows a significant hypsochromic shift with respect to the RT case (3300 cm^{-1}, Table 2), as typically expected for a CT based emission, the energy level of this state is thus estimated at 2.27 eV. To notice that, at low temperature, excitation of **PtL′** at 308 nm, where the truxene ligand is the predominant absorber (see Figure 3a), leads to an emission spectrum markedly different from that obtained upon excitation at 450 nm, where only the Pt(terpy) based ^{3}CT emission is observed, Supporting Information, Figure S2; the difference in the two spectra resides in particular in two peaks emerging at 490 and 530 nm. The comparison with a low temperature phosphorescence spectrum, delayed by 1 ms with respect to fluorescence (Supporting Information, Figure S2), allows to assign these two bands to the phosphorescence of the truxene part of complex **PtL′**. This phosphorescence has a lifetime of 5.8 s (Table 2) and can interestingly be observed upon excitation both at 308 nm and at 440 nm (Supporting Information, Figure S3), where the truxene fragment has no direct absorption. The population of the truxene triplet, clearly observed at 77 K, from the Pt(terpy) based triplet thus appears possible, arising from a $^3Pt \rightarrow {}^3L'$ energy transfer process.

Luminescence of Mononuclear and Dinuclear Complexes. With respect to **Ru** and **Os**, **RuL** and **OsL** display somewhat different luminescence properties: the emission quantum yields of **RuL** and **OsL** are about 40% higher than those of the respective precursors (Table 2) and a shorter lifetime at 77 K is observed for **OsL** (840 ns) with respect to that of model **Os** (2.3 μs); the latter observation is in agreement with data reported for polypyridyl-based Os complexes where one ligand is a polyaromatic group.[43] No truxene based phosphorescence could be detected in these complexes, probably because of the lower spin−orbit coupling constants of the Ru and Os centers with respect to the Pt center (1042 cm^{-1}, 3381 cm^{-1}, and 4481 cm^{-1} for Ru, Os, and Pt, respecively),[33] and because the Ru- and Os-based ^{3}MLCT states of these complexes are much lower in energy than the truxene-based excited states and thus collect almost all the excitation energy, as discussed below.

The characterization of the photoinduced processes that take place between the single metal centers in dyads **Pt−Os**, **Ru−Os**, and in triad **Pt−Ru−Os** has been performed considering **PtL′**, **RuL**, and **OsL** as suitable models for the single component behavior inside the arrays. One should consider that the truxene bridging unit is a "non-innocent" scaffold in these systems; in particular, the interaction Pt-truxene is expected to be significant in the Pt-containing arrays (**Pt−Os** and **Pt−Ru−Os**), since, as already observed for **PtL′**, the truxene triplet level is close in energy to the Pt-based ^{3}CT level. The energy transfer processes that can occur from the truxene singlet, which has an energy content higher than that of all the metallic units in the arrays, will then be discussed in a dedicated section.

From inspection of Figures 3 and 4 it emerges that selective excitation of the Os fragment in the dyads and in the triad is achievable at $\lambda > 550$ nm, whereas excitation at 470 nm produces the following proportions of ^{3}MLCT excited states, 0.8:1 Pt:Os in dyad **Pt−Os**, 1:1 Ru:Os in dyad **Ru−Os**, and 0.8:1:1 Pt:Ru:Os in triad **Pt−Ru−Os**. The RT emission spectra observed upon selective excitation of the Os complex at 600 nm in the dyads **Pt−Os** and **Ru−Os**, in the triad **Pt−Ru−Os**, and in model **OsL** present very similar features: the emission quantum yield is around 1.0×10^{-3} and the lifetime about 20 ns in all cases (Table 2), indicating a weak perturbation of the electronic properties of the $Os(bpy)_2$-truxene type fragment when inserted in the examined arrays. Likewise, the

(42) Baunsgaard, D.; Harrit, N.; El Balsami, M.; Negri, F.; Orlandi, G.; Frederiksen, J.; Wilbrandt, R. *J. Phys. Chem. A* **1998**, *102*, 10007–10016.

(43) Chiorboli, C.; Bignozzi, C. A.; Scandola, F.; Ishow, E.; Gourdon, A.; Launay, J. P. *Inorg. Chem.* **1999**, *38*, 2402–2410.

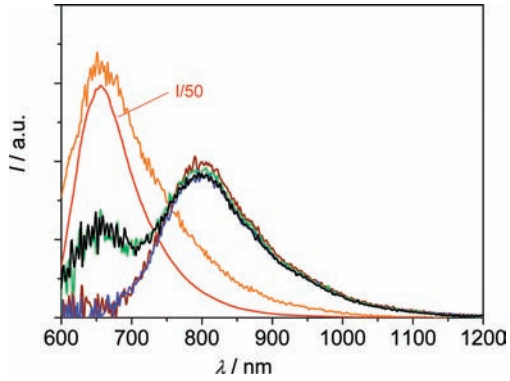

Figure 6. Room-temperature corrected emission spectra of isoabsorbing solutions of **PtL′** (orange), **RuL** (red), **OsL** (brown), **Pt−Os** (blue), **Ru−Os** (green), and **Pt−Ru−Os** (black) in air-free CH_3CN solutions. Excitation at 470 nm. The emission spectrum of **RuL** is divided by 50.

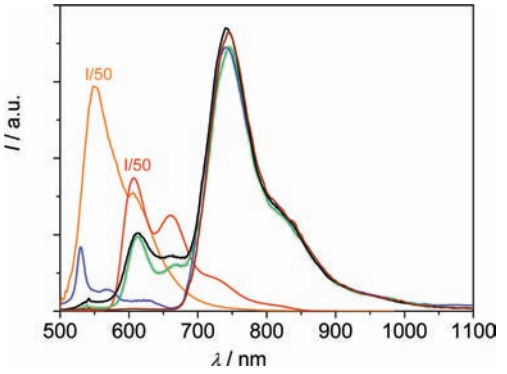

Figure 7. Corrected emission spectra of isoabsorbing solutions at 470 nm of **PtL′** (orange), **RuL** (red), **OsL** (brown), **Pt−Os** (blue), **Ru−Os** (green), and **Pt−Ru−Os** (black) at 77 K in MeOH:EtOH (1:4 v/v). Excitation at 470 nm. The emission spectra of **PtL′** and **RuL** are divided by 50.

lifetime values at 77 K for the Os-based emission of all arrays are similar to that of model **OsL** (Table 2). Excitation at 470 nm of isoabsorbing acetonitrile solutions of the triad, the two dyads and models **PtL′**, **RuL**, and **OsL** leads to the emission spectra displayed in Figure 6; concerned data are listed in Table 2. The luminescence of the Pt unit is completely quenched in the dyad **Pt−Os**, and the luminescence of the Ru unit is reduced to less than 1% that of model **RuL** in dyad **Ru−Os**. The residual Ru-based luminescence in **Ru−Os** has a lifetime of 2.3 ns and is accompanied by a full recovery of the Os-based emission, the latter characterized by a rise time in the excited state decay of 2.5 ns, Table 2. This is indicative of an efficient Ru→Os energy transfer in the dyad, with an evaluated rate constant $k_{en} = 4.3 \times 10^8\ s^{-1}$; $k_{en} = 1/\tau - 1/\tau_0$, where τ is the lifetime of the quenched donor emission and τ_0 is the unquenched donor lifetime.[44,45]

Luminescence of the Target Trinuclear Complex. In triad **Pt−Ru−Os** the weak luminescence at 655 nm (Figure 6) can originate from the overlap of the residual luminescence of both Ru and Pt units because of the substantial overlap of the ^{3}MLCT bands of the two chromophores at RT (see Table 2). It should be pointed out, however, that any Pt-based luminescence in the triad could be excluded, considering that in the simpler system **Pt−Os** the Pt-based luminescence appears completely quenched and there is no reason for a different behavior in the triad where an additional energy collector, the $Ru(bpy)_2$ center, is present. The lifetime of the residual luminescence at 655 nm in the triad is 2.5 ns, very similar to the quenched emission lifetime of the Ru luminescence in **Ru−Os** (Table 2), consistent with a Ru-based nature of the emission. A Ru→Os energy transfer rate constant identical to that derived for **Ru−Os** is thus evaluated also for the triad **Pt−Ru−Os**. These results point to the presence of very efficient energy transfer processes (with efficiencies close to 100%) from the Pt and the Ru units toward the Os unit in both dyads and triad. The Pt→Os energy transfer in the triad could be operative in a single step or via the population of the Ru ^{3}MLCT state.

Figure 7 compares the emission spectra of isoabsorbing MeOH:EtOH (1:4 v/v) solutions at 77 K of the two dyads, the triad and models **PtL′**, **RuL**, and **OsL** excited at 470 nm. At low temperature the luminescence profiles of the three chromophores are well separated, since the Pt based phosphorescence significantly blue-shifts with respect to the RT case and is no more overlapping with the Ru-based emission. It is possible to observe that for **Ru−Os** and **Pt−Ru−Os** the residual luminescence of the Ru center at 615 nm is about 1% that of model **RuL**. Dyad **Pt−Os** shows a peculiar behavior at 77 K: the ^{3}CT Pt based emission at 550 nm is not observed, whereas a structured emission peaking at 530 and 569 nm appears. This emission can be ascribed to the truxene-based phosphorescence, since it closely resembles the delayed **Pt−Os** phosphorescence obtained at low temperature upon excitation at 308 nm (Supporting Information, Figure S4). The process of population of the truxene triplet upon excitation of **Pt−Os** at 470 nm, where the truxene fragment has no absorption, can be operative only via the ^{3}CT of the Pt unit, as already observed for the simpler system **PtL′**. In the case of dyad **Pt−Os**, moreover, the Pt ^{3}CT and the truxene triplet have an almost identical energy, 2.27 and 2.33 eV, respectively, Table 2. In the triad no emission is registered around 550 nm, indicating a fast quenching of both Pt- and truxene-based luminescence; the truxene triplet, if formed, is afterward rapidly depopulated. The Os-based emission intensity is very close to that of model **OsL** in all the examined arrays, Figure 7, indicating that also at low temperature the Os fragment plays as a final collector for the absorbed light energy.

Excitation spectra of dyads **Pt−Os**, **Ru−Os**, and triad **Pt−Ru−Os** recorded at 780 nm at RT and at 760 nm at low temperature, where only the Os phosphorescence is present, confirm the contribution of the Pt and Ru based absorption to the Os emission, evident in all arrays at both temperatures mainly in the region 400−600 nm where the metal-based transitions are operative (Supporting Information, Figure S5).

Cascade Energy Transfer from the Truxene Subunit. The truxene singlet has an energy content higher than those of all the metal-based units present in the arrays: the lowest singlet excited state of ligands **L′** and **L**, in fact, lies at 3.52 and 3.25 eV, respectively, see Table 2. Energy

(44) Sessler, J. L.; Jayawickramarajah, J.; Sathiosatham, M. Energy and Electron Transfer in Supramolecular Systems. In *Encyclopedia of Supramolecular Chemistry*; Atwood, J. L., Steed, J. W., Eds.; CRC Press: Boca Raton, FL, 2004; Vol. *1*, pp 535−545.
(45) Barigelletti, F.; Flamigni, L. *Chem. Soc. Rev.* **2000**, *29*, 1–12.

Scheme 3. Energy Levels of the Excited States[a] and Photoinduced Energy-Transfer Processes in the Examined Complexes

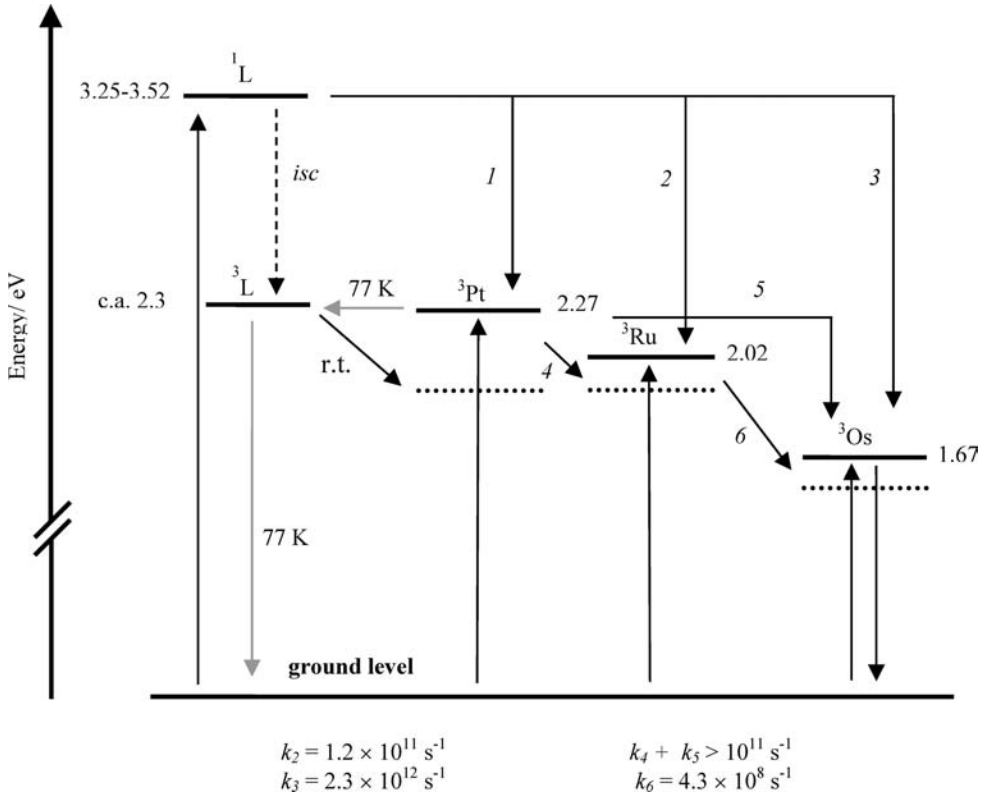

[a] In eV, straight lines for 77 K and dotted lines for RT values.

transfer processes from ^{1}L toward Pt, Ru, and Os centers are thus all possible, as depicted in Scheme 3; the processes ^{1}L′ → ^{3}Pt, ^{1}L → ^{3}Ru, and ^{1}L → ^{3}Os are exoergonic by 1.15, 1.23, and 1.58 eV, respectively. Moreover, the triplet state of the truxene fragment lies at higher energy than the Pt(based) triplet at RT (see Scheme 3) and also the process ^{3}L → ^{3}Pt can take place. To gain insight into the truxene-based photophysics, the emission of mononuclear complexes **PtL′**, **RuL**, **OsL** and of dyads and triad, upon predominant excitation of the truxene singlet excited state, has been exploited considering as models the precursors **Pt**, **Ru**, and **Os**, that lack the truxene fragment (Chart 1). From Figure 3a one sees that at 308 nm, 80% of the light absorbed by **PtL′** goes on the truxene **L′**. Likewise, a comparison between the absorption spectra of **L**, **RuL**, **OsL** and of models **Ru** and **Os**, as reported in Figure 3b−c, leads to identify another wavelength, 367 nm, where the truxene ligand (**L** in these cases) absorbs 95% and 85% of the photons absorbed by **RuL** and **OsL**, respectively. For this reason, 367 nm is the wavelength of choice for the predominant excitation of the truxene core also in the two dyads and in the triad, where the reference ligand is again the bipyridine containing truxene **L**. Precursors **Pt**, **Ru**, and **Os**, while useful models for the absorption properties of the truxene-containing complexes, are not good models for the metal-based emission of the same complexes and the arrays, since they show different emission quantum yields if compared with their respective truxene-containing derivatives, as already observed. Therefore, to use appropriate metal-based emissions as reference, we chose the Pt-based emission of **PtL′**, selectively excited at 470 nm, the Ru-based emission of **RuL**, selectively excited at 470 nm, and the Os-based emission of **OsL** upon selective excitation at 600 nm.

Comparison of the luminescence of isoabsorbing solutions at 308 nm of **L′** and complex **PtL′**, together with the emission spectrum of **PtL′** excited at 470 nm (Supporting Information, Figure S6) shows that the residual fluorescence of the truxene ligand in **PtL′** can be roughly estimated around 0.1−0.3% with respect to that of model **L′**, whereas the Pt ^{3}CT luminescence yield is quite completely recovered. This allows to estimate a rate constant for the quenching of the ligand excited state of about 5×10^{10} s^{-1} and an efficiency close to 100%. The Pt-based triplet is thus the final collector for the energy absorbed by the ligand in **PtL′** at RT, if the process is either a direct ^{1}L′→^{3}Pt energy transfer or, most likely, a ^{3}L′→^{3}Pt energy transfer process consequent to the population of the ligand triplet because of an enhanced intersystem crossing promoted by the heavy Pt atom (see Scheme 3).

A similar comparison for **RuL** and **OsL** with ligand **L** upon excitation at 367 nm revealed that the fluorescence of the ligand is almost completely quenched also in these two complexes and the Ru-based and the Os-based emissions are almost completely recovered.

Figure 8 shows the emission spectra of dyads **Pt−Os** and **Ru−Os**, triad **Pt−Ru−Os**, and ligand **L** excited at 367 nm, together with the Pt-based luminescence of **PtL′** excited at 470 nm, the Ru-based luminescence of **RuL** excited at 470 nm, and the Os-based luminescence of **OsL** excited at 600 nm; in the figure the spectra are scaled according to the emission quantum yields. It is evident that (i) the fluorescence of the truxene ligand is completely quenched in all the arrays; (ii) no Pt-based luminescence is

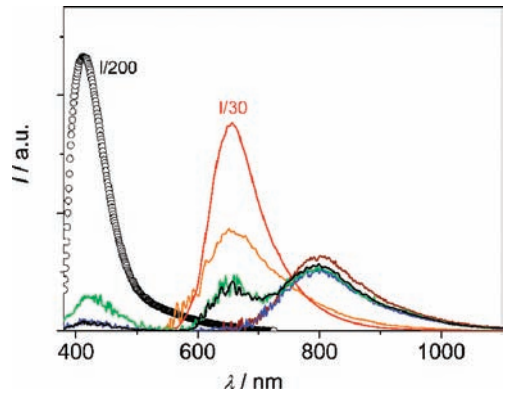

Figure 8. Room-temperature corrected emission spectra of CH_3CN solutions of **Pt−Os** (blue), **Ru−Os** (green), and **Pt−Ru−Os** (black) excited at 367 nm, **PtL′** excited at 470 nm (orange), **RuL** excited at 470 nm (red), and **OsL** excited at 600 nm (brown). The emission spectrum of a CH_2Cl_2 solution of **L** (open cirles) excited at 367 nm is also reported. Air-free solutions. Spectra scaled according to the emission quantum yields. The emission spectra of **L** and **RuL** are divided by 200 and 30, respectively.

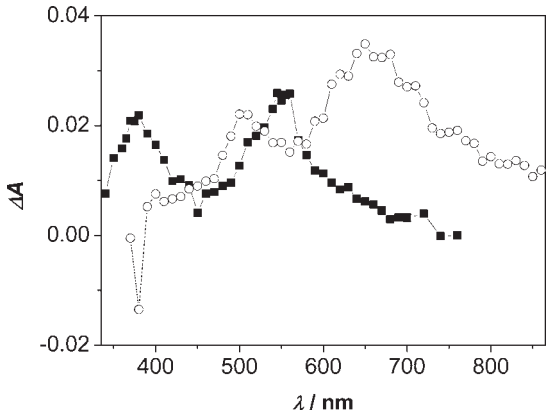

Figure 9. End-of-pulse transient absorption spectra of **L′** (black squares) and **L** (open circles) in air-free CH_2Cl_2 solutions. Excitation at 266 nm.

observed in **Pt−Os** and in the triad, whereas (iii) a residual Ru-based emission is observed in both dyad **Ru−Os** and triad. With respect to point (i) the fluorescence of **L** is reduced to less than 0.1% in **Pt−Os**, **Ru−Os**, and **Pt−Ru−Os**. This allows to evaluate rate constants for the quenching of the ligand fluorescence $\geq 1 \times 10^{12}$ s^{-1}. Taking into consideration the rate constants for the $^1L \rightarrow {}^3Ru$ and the $^1L \rightarrow {}^3Os$ transfer processes (processes *2* and *3* in Scheme 3) observed in the monometallic systems **RuL** and **OsL** (1.2×10^{11} s^{-1} and 2.3×10^{12} s^{-1}, respectively) one can thus conclude that the leading process in all the multichromophoric arrays is energy transfer from the ligand singlet to the Os based triplet. This accounts for about 80−90% of the transferred energy, in accordance with the large driving force of the $^1L \rightarrow {}^3Os$ process (Scheme 3). In turn, this means that when Os is present only 10−20% of the energy transferred from the ligand contributes to the population of the Pt-based and Ru-based triplets (processes *1* and *2*). Actually, in the Pt-containing arrays, no Pt-based emission is detected and in the Ru-containing arrays a residual Ru-based emission can be observed, because of the slow process $^3Ru \rightarrow {}^3Os$ (k ca. 4×10^8 s^{-1}, process *6*). Figure 8 confirms that the yield of the Os-based emission upon prevalent excitation of the ligand is around 80%−90% that of the model in **Pt−Os**, **Ru−Os**, and **Pt−Ru−Os**.[46] The discussion on the mechanisms of the several metal-based energy transfer processes that occur in the triad is beyond the scope of the present work.

In summary, in the dyads and in the triad, from the luminescence data we have obtained evidence for fast and efficient energy transfer processes that funnel energy toward the low-lying Os-based triplet excited state. The population of the truxene triplet in these systems at RT seems disfavored by the competition with the transfer of energy toward the Os-center driven by a high energy gap. At low temperature the shift at higher energy of the Pt ^3CT level makes the process of population of the truxene triplet feasible also in the Os-containing dyad **Pt−Os**, as observed.

Transient Absorption. To get further insights in the triplet dynamics we performed transient absorption measurements in the nanosecond range for selected compounds. For the reasons mentioned above, complex **PtL′** has been chosen to understand the role of the truxene ligand in the Pt-based photophysics, and **L′** and **Pt** were considered as reference compounds. The samples were probed by using excitation at 266 nm, to ensure a suitable absorption of ligand **L′**, the percentage of absorbance of **Pt** and **L′** in **PtL′** at this wavelength being 65% and 35%, respectively (Figure 3a). The same analysis was performed on ligand **L**, for comparison with ligand **L′**. Figure 9 compares the end-of-pulse transient absorption spectra of ligands **L′** and **L**: the two spectra have similar profiles with two absorption bands considerably red-shifted in the case of **L**. The lifetimes evaluated for **L′** and **L** are 61 and 58 μs, respectively, in air-free dichloromethane solutions, and 2.5 and 1.0 μs in aerated conditions (the time evolution of the transient absorbance of the two ligands in air-free conditions is reported in Supporting Information, Figure S7). On the basis of the observed features, these spectra can be safely assigned to the lowest triplet excited states of the ligands.[20]

Figure 10 compares the end-of-pulse spectra of solutions of **PtL′**, **Pt**, and **L′**, prepared so that **Pt** and **L** absorb the same amount of photons as does the corresponding unit in **PtL′**. The spectral profile of **Pt** resembles that reported in literature and attributed to ^3Pt,[31,39,47] with the obtained lifetime of 335 ns being in nice agreement with the phosphorescence lifetime of **Pt** (310 ns, Table 2), confirming the nature of the transient absorbing state; the time evolution of the differential absorption is shown in Supporting Information, Figure S8a. **PtL′** displays an end-of-pulse spectrum markedly different from that of **Pt**,

(46) The rates of the energy transfer processes depend not only on the distance between the partners but also on the spectral overlap factors. The triad **Pt-Ru-Os** is not perfectly symmetric as it appears, since from preliminary calculations it was found that there is a certain degree of conformational freedom in the array, because of the possibility of rotation of the metal-connected bipyridyl units around the lateral truxene linked triple bonds; a distribution of conformations can thus lead to different mean metal to metal distances. It should also be considered that not only Förster mechanism can be involved in the metal based energy transfer processes but also the conjugated truxene bridge very likely renders the through-bond Dexter mechanism operative.

(47) Castellano, F. N.; Pomestchenko, I. E.; Shikhova, E.; Hua, F.; Muro, M. L.; Rajapakse, N. *Coord. Chem. Rev.* **2006**, *250*, 1819–1828.

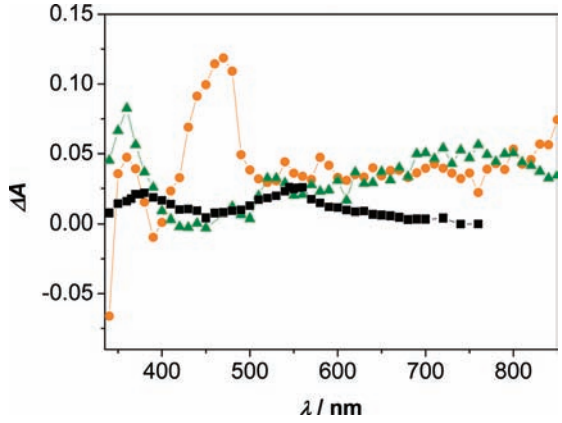

Figure 10. End-of-pulse transient absorption spectra of **PtL′** (orange circles) and **Pt** (green triangles) in CH_3CN solutions and of **L′** in CH_2Cl_2 solution (black squares). Excitation at 266 nm.

with a bleaching below 350 nm, an intense positive band at 470 nm, and a broad absorption above 800 nm, see Figure 10. A lifetime of 23.5 ns is evaluated as a single exponential at any wavelengths (Supporting Information, Figure S8b), nicely coincident with that of the room-temperature ^{3}CT luminescence of **PtL′** (22.0 ns, Table 2); the transient spectrum can thus be attributed to this state, and the different spectral features observed in this case with respect to the transient absorption spectrum of **Pt** confirm the different nature of the two Pt-based triplets. It should be pointed out that in our case the transient absorption of **PtL′** is dominated by the Pt-centered triplet, contrary to some reported cases of Pt-acetylide derivatives where the end-of-pulse transient absorption spectrum matches the features of the lowest ligand based triplet.[30,31] This could be explained by considering that in the mentioned cases, the energy difference between the Pt- and ligand based triplet states at RT might be lower than in our case. Actually, in complex **PtL′** clear-cut truxene triplet features are apparent only at 77 K, where the destabilization of the Pt ^{3}CT level pushes it close in energy to the truxene triplet.

Conclusions

Here we have reported on the synthesis, characterization, and study of the photophysical properties of a newly designed star-shaped trimetallic architecture based on a truxene platform, linked to a terpyridine-Pt(II) ethynylene unit and two bipyridine complexes of Ru(II) and Os (II). The Pt, Ru, and Os units are connected to the rigid platform via acetylene linkers and develop in three diverging directions in space. From a photophysical viewpoint the truxene core has not only a structural function but is a photoactive component that enriches the photophysics of the derived arrays. The luminescence data, analyzed in the light of the properties of the reference mono- and binuclear complexes, evidenced fast energy transfer processes leading to the final population of the Os-based excited states. Upon photoexcitation of the truxene singlet a fast ^{1}L→^{3}Os energy transfer occurs with high efficiency, in accord with the large driving force of the ^{1}L→^{3}Os process. A small fraction of the excitation energy (10−20%) is funneled to the Os center via an energy cascade that involves, in turn, the Pt and Ru ^{3}CT levels. The nature of the CT triplet in the **PtL′** system is influenced by the presence of the conjugated truxene scaffold, and at RT this low lying state is the final collector of the absorbed energy, as confirmed by transient absorption experiments. At low temperature, the interaction between the truxene-based and the Pt-based triplet states is facilitated by the closeness in energy of the two levels. Moreover, the truxene-based triplet, whose population is probably enhanced by the proximity of the Pt atom, is not depopulated by energy transfer toward the Pt-based triplet; to notice that an inverse ^{3}Pt→^{3}L process is feasible. As a result, in the Pt-containing complexes the truxene phosphorescence can be observed, also upon excitation of the Pt-based triplet. These observations improve the knowledge on the truxene photophysics in view of its utilization as a suitable structural motif in supramolecular architectures.

The two synthesized truxene ligands moreover showed interesting photophysical properties, such as high emission quantum yields and well resolved phosphorescence, characteristics that can be usefully employed in optoelectronic or sensing applications.

Acknowledgment. Funding from CNR of Italy (PM. P04.010, Project MACOL), MIUR (FIRB RBIP0642YL, Project LUCI; FIRB RBIP0642YL, Project NODIS), and the Centre National de la Recherche Scientifique are acknowledged. We also thank le Ministère de la Recherche Française et des Nouvelles Technologies for a fellowship to S.D. B.V., A.B., and F.B. (Bologna) thank colleague Lucia Flamigni for helpful discussion, and R.Z. (Strasbourg) warmly thanks Johnson Matthey PLC for a loan of precious metal salts.

Supporting Information Available: Characterization of the **Pt** and **PtL′** complexes (Table S1 and Figure S1), additional spectroscopic characterization of **PtL′** and arrays (Figures S2−S6), time evolution of the transient absorption of ligands **L′** and **L** (Figure S7), time evolution of the transient absorption of the **Pt** and **PtL′** complexes (Figure S8). This material is available free of charge via the Internet at http://pubs.acs.org.